Fatigue Testing and Analysis of Aluminum Welds under In-Service Highway Bridge Loading Conditions

Reid Coughlin[1] and Scott Walbridge, Ph.D., P.Eng., M.ASCE[2]

Abstract: For the fatigue design of aluminum structures, most applicable international codes specify fatigue-resistance (S-N) curves with slopes that vary, depending on the detail category. This complicates the selection of appropriate damage equivalence factors for use in highway bridge applications. The existing codes also differ in their treatment of high cycle fatigue, with single-slope S-N curves specified in some cases and multislope curves specified in others. In this paper, a recent investigation conducted to examine the fatigue behavior of aluminum welds under in-service highway bridge loading conditions is summarized. Specifically, calculations performed to establish damage equivalence factors for aluminum for use with the AASHTO and Canadian Standards Association (CSA) CAN/CSA-S6 codes are first reviewed. Following this, small-scale fatigue tests of aluminum welds under simulated highway bridge loading conditions are described. A fracture mechanics model is then validated by comparison with the test results and used to perform simulations encompassing a wider range of loading conditions. On the basis of this work, the adequacy of the current design provisions is discussed and possibilities for further extending the employed methodology are identified. **DOI: 10.1061/(ASCE)BE.1943-5592.0000223.**

CE Database subject headings: Aluminum; Fatigue; Highway and road structures; Highway bridges; Welding; Load factors.

Author keywords: Aluminum; Fatigue; Highway and road structures; Bridges; Welds; Overloads.

Introduction

The use of aluminum in highway bridges can provide efficient solutions in certain cases. Life-cycle cost analyses have shown the economic benefits of using corrosion-resistant aluminum for the replacement of existing bridge decks (Arrien et al. 2001; Siwowski 2006). The rehabilitation of existing bridges by replacing aging concrete decks with new extruded aluminum ones, can significantly increase the live load capacity attributable to the resulting reduction in the dead load. The relative ease of transportation and erection of aluminum bridge components also facilitates accelerated construction applications, as all or part of the structure can be shipped and installed on-site (Das and Kaufman 2007).

The long-term performance of aluminum structures can be highly dependent on the fatigue behavior of the welds. In welded aluminum structures, the heat generated during the welding process can reduce the material strength in the heat-affected zone by removing the effects of cold-working. In aluminum and steel structures, initial defects, tensile residual stresses, and the stress concentration attributable to the local change in geometry are known to lead to a reduced fatigue performance in the vicinity of the welds (Menzemer 2000).

Large databases of test results have been used to establish the current fatigue design provisions for aluminum welds. Fatigue test results on specific weld details have been reported in several studies (Maddox and Webber 1977; Maddox 1995; Mazzolani and Grillo 1995). Others have compiled test results and discussed the development of the current fatigue design provisions (Menzemer and Fisher 1995; Jaccard et al. 1995; Soetens et al. 1995; Maddox 2003), which commonly employ fatigue-resistance (S-N) curves and the detail category approach.

For the current study, Fig. 1 provides a comparison of design S-N curves from several standards for one fatigue detail—a non-load-carrying fillet welded transverse stiffener. Differences between the curves are apparent in this figure. Multislope curves are used in most cases, in which the high cycle portion of the S-N curve has a shallower slope, indicating that damage under variable amplitude (VA) loading beyond the constant amplitude fatigue limit (CAFL) occurs at a reduced rate. The Aluminum Association (AA) design manual (ADM) (AA 2010) employs the simpler approach of extending the S-N curve beyond the CAFL at the same slope. AASHTO (2007) also uses this approach, with a similar set of single-slope S-N curves on the basis of ADM 1986 (Menzemer and Fisher 1995). Although the AASHTO (2007) and ADM (AA 2010) curves have no slope change at the CAFL, they both have an upper limit equal to the stress range at $N = 10^5$ cycles. This is shown in Fig. 1 as a horizontal line for the ADM (AA 2010) curve.

One reason for differences in the current design provisions beyond the CAFL is that most of the available fatigue data for aluminum welds has come from tests conducted under constant amplitude (CA) loading conditions. Several references have identified aluminum weld fatigue behavior under VA loading as an area that needs further study (Voutaz et al. 1995; Menzemer 2000; Maddox 2003). In comparison with the data for welded steel structures under such loading conditions, the available data for welded aluminum structures remains limited.

Regardless of whether-single slope or multislope S-N curves are used, most standards [with the exception of the International Institute of Welding recommendations (Hobbacher 2005)] use S-N curves for aluminum with slopes in the low cycle domain that vary with the detail category. This can complicate the establishment of

[1]Dept. of Civil and Environmental Engineering, Univ. of Waterloo, 200 University Ave. West, Waterloo, Ontario, Canada N2L 3G1.

[2]Dept. of Civil and Environmental Engineering, Univ. of Waterloo, 200 University Ave. West, Waterloo, Ontario, Canada N2L 3G1 (corresponding author). E-mail: swalbrid@civmail.uwaterloo.ca

Note. This manuscript was submitted on October 1, 2010; approved on January 11, 2011; published online on January 13, 2011. Discussion period open until October 1, 2012; separate discussions must be submitted for individual papers. This paper is part of the ***Journal of Bridge Engineering***, Vol. 17, No. 3, May 1, 2012. ©ASCE, ISSN 1084-0702/2012/3-409–419/$25.00.

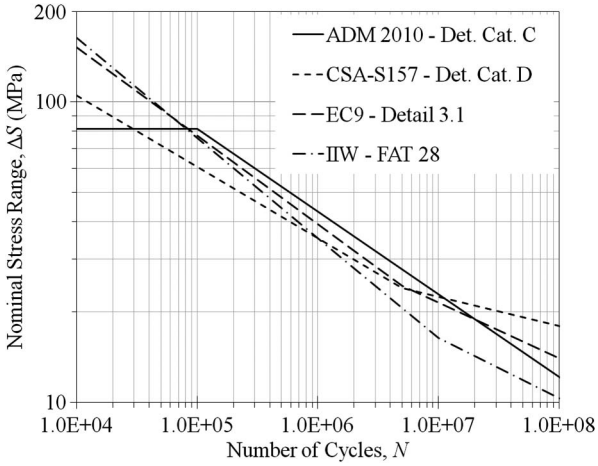

Fig. 1. Design S-N curves for non-load-carrying fillet welded transverse stiffeners

design factors for applications such as highway bridge design, in particular when these factors are dependent on the assumed S-N curve-slope.

In many highway bridge design codes, the calculated design stress ranges are multiplied by a damage equivalence factor, for example, to account for differences in the fatigue damage attributable to the code truck and the expected real traffic. In the AASHTO (2007) and Canadian Standards Association (CSA 2006) CAN/CSA-S6 codes, damage equivalence factors have been established for use with S-N curves that have a single-slope of $m = 3.0$. Although suitable for steel, the appropriateness of these factors for use with aluminum S-N curves with slopes $m > 3.0$ is questionable.

A new chapter of the CAN/CSA-S6 code for the design of aluminum highway bridge structures is currently under development. To further study the issues raised in the preceding paragraphs within the context of the development of this new code chapter, an investigation was recently undertaken (Coughlin 2010), the results of which are summarized in this paper. First, this paper reviews calculations performed to establish damage equivalence factors for aluminum for use with the AASHTO and CAN/CSA-S6 codes. Following this, small-scale fatigue tests of aluminum welds under simulated highway bridge loading conditions are described. A fracture mechanics model is then validated by comparison with the test results and used to perform simulations encompassing a wider range of influence lines and bridge spans. On the basis of this work, the adequacy of the current design provisions is discussed.

The scope of the fatigue testing and fracture mechanics analysis presented in this paper is limited to a single detail category and analyzed by using a deterministic analytical model. However, this methodology can be extended to other detail categories, large-scale specimens, and a probabilistic analytical format, as discussed in the Conclusions.

Fatigue Damage Equivalence Factors

Correction factors are employed in a number of highway bridge codes for relating the fatigue damage attributable to the real traffic to that predicted by a simplified design model. In AASHTO (2007) and CAN/CSA-S6 (CSA 2006), this objective is achieved with two factors—a damage equivalence factor, $\gamma = 0.75$ in AASHTO or $\lambda = 0.52$ in CAN/CSA-S6, and a second factor, n in AASHTO or N_d in CAN/CSA-S6, to consider the expected number of stress cycles per truck passage.

The basis for $\gamma = 0.75$ in AASHTO (2007) is provided in (Moses et al. 1987), wherein a fatigue design truck is proposed with a gross vehicle weight (GVW) that is 0.75 times that of the code truck for static design. This factor was determined by taking the GVW histogram from a survey of 27,513 trucks (Snyder et al. 1985) and calculating the equivalent weight of the fatigue design truck using the following expression:

$$W_{\text{eq}} = \left(\sum f_i \cdot W_i^3\right)^{1/3} \tag{1}$$

where f_i = frequency associated with the GVW, which is represented by W_i. This formula is a rearrangement of the well-known Miner's sum with $m = 3.0$ assumed as the slope of the S-N curve.

In CAN/CSA-S6, the derivation of this factor for steel involved consideration of the differences in the Canadian and American real traffic, code trucks, and dynamic load allowances (DLAs). The derivation was verified by performing analyses of histograms for various load effects provided in the CAN/CSA-S6 calibration report (Agarwal et al. 2007).

For the fatigue design of aluminum structures, ADM (AA 2010) uses single-slope S-N curves, with slopes ranging from $3.42 \leq m \leq 6.85$. The corresponding AASHTO (2007) slopes range from $3.42 \leq m \leq 6.45$. To evaluate the appropriateness of the current damage equivalence factors in AASHTO (2007) and CAN/CSA-S6 (CSA 2006) for use with S-N curves in which $m > 3.0$, a methodology was employed that has the advantage over the use of Eq. (1)—or variations thereof—and can account for the effects of varying axle group weights and truck configurations for different bridge structure (or component) spans and influence lines. The employed methodology is the same one used to calibrate the damage equivalence factor, λ_1, in the Swiss steel structures code [Swiss Society of Engineers and Architects (SIA) 2003]. An overview can be found in Hirt et al. (2006).

Calculation Inputs and Methodology

The following information is required to calculate the damage equivalence factor by using the employed methodology: (1) a code truck model, (2) real traffic data for the region of interest, (3) influence lines for various critical locations in bridges, and (4) a design service life and expected traffic volume. In fact, if the calculation is for a single-slope S-N curve, the fourth item is not required, because the result is independent of the fatigue life (N).

The code truck models employed in the current calculations were the AASHTO (2007) HS20-44 and CAN/CSA-S6 (CSA 2006) CL-625 code trucks [see Fig. 2(a)].

For the CAN/CSA-S6 λ factor calculation, axle weight and spacing data for 10,198 trucks measured in Ontario in 1995 (Agarwal et al. 2007) was used to represent the real traffic. For the AASHTO γ factor calculation, GVW data from (Snyder et al. 1985) was employed. These data included weigh-in-motion (WIM) measurements from 30 sites in seven states. Of the 27,513 trucks weighed in this survey, 25,901 group within six truck categories defined in Moses et al. (1987). Snyder et al. (1985) report their results as GVW histograms for 11 truck types. Given these histograms, each of the 11 truck types was assigned idealized axle weights, defined as a percentage of the GVW per axle, in accordance with the six categories defined in Moses et al. (1987). The resulting U.S. and Ontario GVW histograms are compared in Fig. 2(b). They have some similarities. However, the

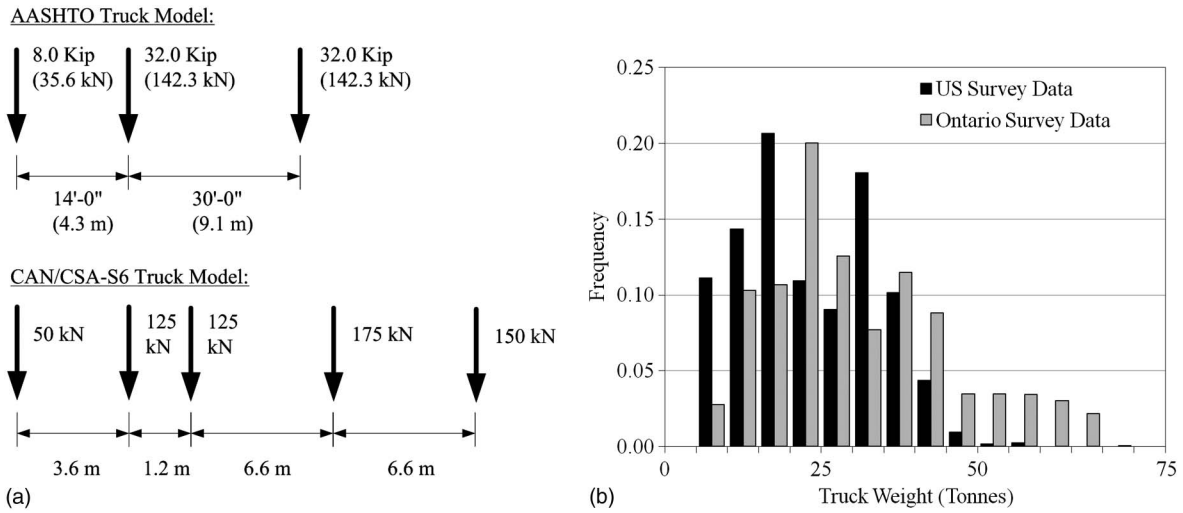

Fig. 2. United States and Canadian damage equivalence factor calculation inputs: (a) code truck models; (b) gross vehicle weight histograms

histogram from Agarwal et al. (2007) is clearly skewed to the right, indicating larger percentages of eavier trucks.

The following influence lines were used in the damage equivalence factor calculation: positive moment at the midspan for 1-, 2-, and 5-span girders (ps-m, p2tr-m, and p5tr-m, respectively); negative moment at the intermediate support for 2- and 5-span girders (p2tr-a and p5tr-a, respectively); and support reaction for 1- and 2-span girders (ps-r and p2tr-r, respectively). Equal spans were assumed in all cases, except that for the 5-span girders, 20% shorter end spans were assumed.

Calculations were performed by using the seven examined influence lines and considering spans from $L = 2$ to 60 m. These spans were chosen to cover a wide range of bridge components, from deck elements up to medium span bridge girders. A program was written in FORTRAN 95 to perform the analysis. In brief, the calculation procedure involves generating load effect range histograms for each span and influence line attributable to the real traffic database (by moving each truck in the database across the influence line in succession and calculating stress ranges by using the rainflow method), and then comparing them to corresponding design load effect ranges attributable to a single passage of the code truck. To do this, the vertical positions of the S-N curve required to produce a damage index, $D = 1.0$ (on the basis of Miner's sum) under the real traffic histogram and under CA loading at the design load effect range are characterized by M as follows:

$$\log(N) = \log(M) - m \cdot \log(\Delta S) \tag{2}$$

where ΔS = nominal stress range (assumed to be proportional to the load effect range). Once the two values of M are calculated (M_{real} for the real traffic histogram and M_{code} for the CA code truck range), the damage equivalence factor is calculated as

$$\gamma(\text{or } \lambda) = \left(\frac{M_{\text{real}}}{M_{\text{code}}}\right)^{1/m} \tag{3}$$

By using this approach, results can be obtained without knowing the actual nominal stress ranges, because the factor relating the load effects to the nominal stresses cancels out in Eq. (3). Further details regarding this calculation procedure are provided by Coughlin (2010).

Typical Calculation Results

Fig. 3(a) and 3(b) presents typical damage equivalence factor calculation results on the basis of the procedure described in the previous section. In Fig. 3(a), results are presented for the AASHTO γ factor calculation for $m = 3.0$ (i.e., for steel). The results for the examined spans and influence lines vary, but indicate an average value for this parameter of approximately 0.75. This demonstrates that the employed procedure and U.S. GVW database yield results that are consistent with the current code value for the γ factor.

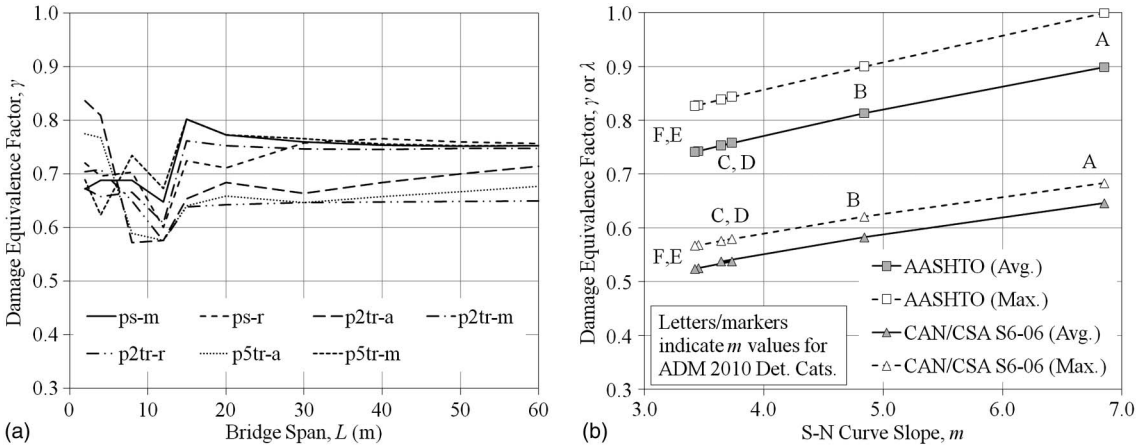

Fig. 3. Damage equivalence factor calculation results: (a) results for steel ($m = 3.0$); (b) results for aluminum detail categories

J. Bridge Eng. 2012.17:409-419.

In Fig. 3(b), the results of similar calculations for $m = 3.45$ to 6.85 are summarized in plots of γ versus m. To generate the plotted curves, the average and maximum values of γ for all of the influence lines between spans of 15 and 60 m were calculated for each value of m.

As shown in Fig. 3(b), the plotted data points correspond with the m values for detail categories A to F in ADM (AA 2010). The AASHTO (2007) m values differ somewhat from these. However, the ADM (AA 2010) S-N curves were calibrated with more recent data (Menzemer and Fisher 1995), and are thus assumed to be more up-to-date. In any case, the curves in Fig. 3(b) can be used to determine suitable γ values for any value of m within the investigated range.

In Fig. 3(b), similar curves are plotted of the λ factor for use in CAN/CSA-S6. In both cases, the average curves appear to converge on the current values for steel at $m = 3.0$. For ADM (AA 2010) detail categories C to F, average damage equivalence factors only slightly larger than the steel factors are calculated. For detail categories A and B, or m greater than ~4.5, the calculated factors are substantially larger. On this basis, it can be concluded that a higher damage equivalence factor may be appropriate for these cases.

Additional calculations employing variations of this methodology are described by Coughlin (2010) for the multislope S-N curves from CSA-S157 (CSA 2005) and to investigate the effects of periodic overload trucks and simultaneous vehicle crossings. In the paper by Coughlin (2010), further studies are recommended, employing larger, more recent traffic databases and a more sophisticated simultaneous vehicle crossing model. However, the γ and λ curves in Fig. 3(b) are immediately useful, as they are expected to provide a level of safety for the fatigue design of aluminum bridge structures consistent with that provided by the current values for steel.

Table 1. Fatigue Test Program

ΔS or ΔS_{eq}	R	Loading	Specimens
MPa	—	—	#
70, 80, 90, 100, 120, 150, 170, 200	−1.0	CA	8
60, 70, 80, 90	0.1	CA	4
50, 60, 70, 80	0.4	CA	4
20, 30, 40, 60, 75	—	ps-m-40	9
30, 75	—	ps-r-15	6

Note: Reported stress ranges are target values. Actual, tested stress ranges are plotted in Fig. 6.

Laboratory Testing of Aluminum Welds

Fatigue Test Program

The testing program conducted for this investigation included the fatigue tests of 31 small-scale, non-load-carrying fillet welded transverse stiffener details under CA and VA loading conditions (see Table 1). All specimens were loaded axially (see Fig. 4). Testing under CA loading was conducted at R-ratios of −1.0, 0.4, and 0.1, and at various stress ranges, ΔS.

Testing under VA loading was conducted by using two stress histories derived from the 1995 Ontario traffic data (Agarwal et al. 2007) to simulate in-service loading conditions. Given this data, two 200 peak sample histories were randomly extracted from the larger histories generated for the CAN/CSA-S6 damage equivalence factor calculation. Specifically, the following cases were considered: the midspan moment of a 40 m girder (ps-m-40) and the support reaction of a 15 m girder (ps-r-15). The two stress histories are compared in Fig. 5. For the ps-m-40 history, the passage of each truck generally results in only a single load cycle, because the bridge span is much longer than the truck length. For the ps-r-15 history, each axle load tends to cause a small cycle as it comes on or off the girder. The result is that for the first history, the stress ratio, R, is approximately constant, whereas for the second, this parameter varies considerably.

The test specimens were fabricated from 3/8 in. (9.5 mm) thick 6061-T651 aluminum plates with transverse attachments fillet welded at the midheight. All welded joints were fabricated by gas metal arc welding (GMAW) with 5356 aluminum weld metal filler. Eight 300-mm wide stiffened panels were fabricated and then saw-cut into five 50-mm wide specimens per panel.

Fatigue testing of all specimens was undertaken under load control by using an MTS 810 materials testing system (load capacity ±100 kN), equipped with hydraulic control, hydraulic power, and hydraulic actuated grips. The duration of each test was governed by the specimen's fatigue life at a cycling frequency of 8 Hz;

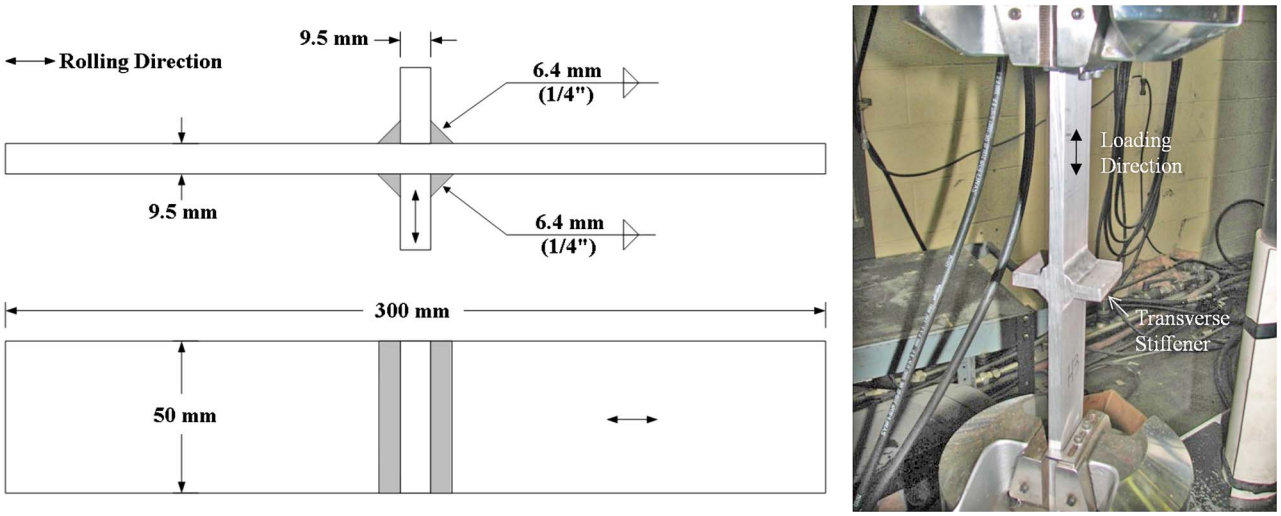

Fig. 4. Fatigue specimen geometry and test setup

J. Bridge Eng. 2012.17:409-419.

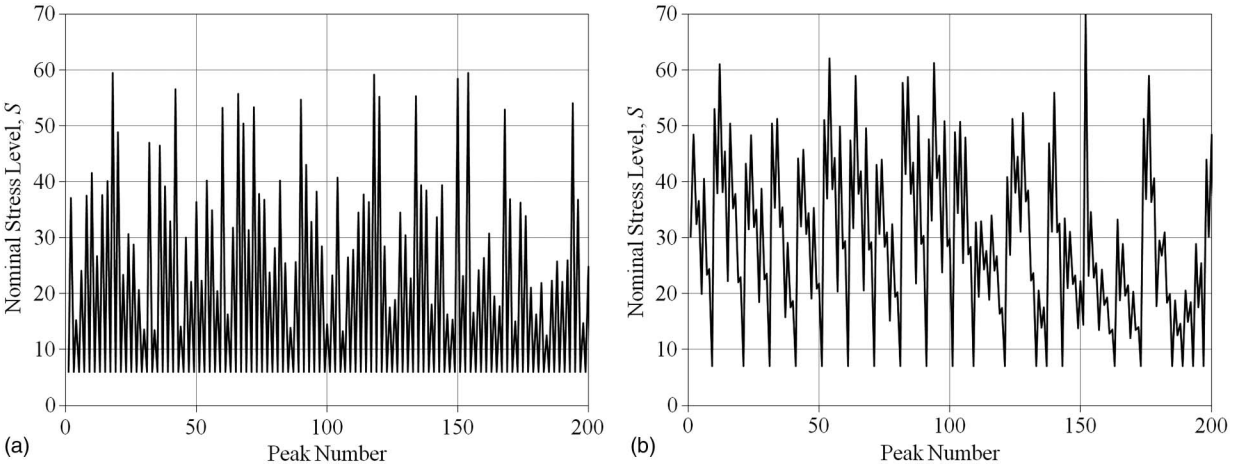

Fig. 5. Simulated in-service load histories: (a) ps-m-40 loading; (b) ps-r-15 loading

the only exceptions to this test speed were the VA loading tests at 16.5 MPa and 30 MPa, which were conducted at 28 Hz. The testing frequencies at these lower stress ranges were increased to facilitate the extended duration of testing.

Fatigue Test Results

Fig. 6 presents a log-log S-N plot of the fatigue test results under CA and VA loading, along with the ADM (AA 2010) detail category C design curve, for comparison purposes. The CA test results for $R = 0.1$ and 0.4 show limited scatter and generally fall along straight lines on the S-N plot. In contrast, noticeable scatter is apparent, in the CA test results for $R = -1.0$. The test results for $R = -1.0$ and 0.1 all lie above the ADM (AA 2010) detail category C design curve. However, some of the test results for $R = 0.4$ fall below the curve.

The VA loading results are plotted by using an equivalent stress range on the basis of Miner's sum with $m = 3.64$, which is the slope of the ADM (AA 2010) detail category C design curve

$$\Delta S_{\text{eq}} = \left(\frac{\sum n_i \cdot \Delta S_i^m}{\sum N_i}\right)^{1/m} \tag{4}$$

The results at the higher stress levels ($\Delta S \approx 75$ MPa) show limited scatter and little difference between the two load histories. The results at the lower stress levels ($\Delta S \approx 30$ MPa) show more scatter and a noticeable difference in fatigue performance for the two histories.

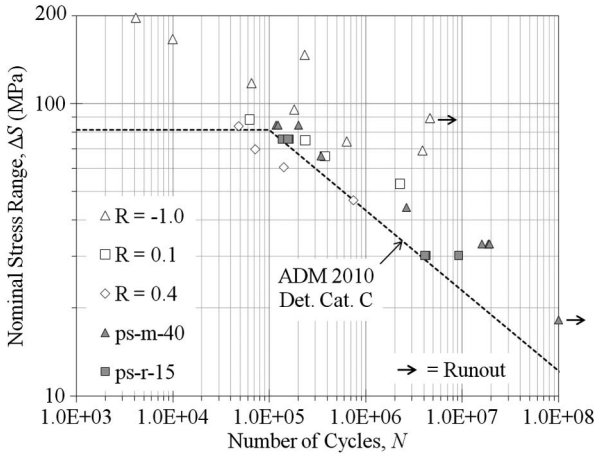

Fig. 6. Fatigue test S-N results

Materials Tests

Static tension tests were performed in accordance with ASTM (2004) on three as-received (T651) and two annealed (O) coupons. The annealed coupons were heat treated, in accordance with ASTM (2009). The resulting average elastic modulus (E), yield (σ_y), and ultimate strength (σ_u) values are summarized in Table 2. The difference in σ_y and σ_u for the two tempering cases (T651 and O) is clear in this table—both values are much higher for the as-received coupons. The yield point was clearly defined for the as-received coupons. For the annealed coupons, the yield point was not clearly defined; thus, the 0.2% rule was used to determine the yield stress.

Cyclic materials tests were conducted to determine the cyclic Ramberg-Osgood material constants (K' and n') for the T651 and O tempers. These tests were performed on polished smooth cylindrical, variable width specimens that have a 5.0 mm diameter within the 7.6 mm (0.3 in.) gauge length. The testing was conducted by imposing strain cycles (10 per strain level) at $R = -1.0$ in increments of 0.1% up to $\pm 1.0\%$ strain and then back down to $\pm 0.1\%$ strain, and repeating until the load stabilized for each strain level. The constants K' and n' were then determined by fitting the cyclic Ramberg-Osgood model to the stabilized stress-strain data. The average results of the cyclic materials tests are summarized in Table 2.

Microhardness measurements of the T651 and O temper base metal, and the HAZ and the weld metal (WM) itself, were performed in accordance with ASTM (2003). Average Vickers hardness (HV) numbers of 109.8 and 51.0 were obtained for the T651 and O temper base metal, respectively. The lower hardness for the O temper is consistent with the expected softening effect attributable to the annealing. Microhardness measurements also were taken at multiple locations along a fatigue specimen

Table 2. Tested and Estimated Material Properties

	Material			
	T651	O	HAZ	Units
Vickers hardness	109.8	51.0	74.8	HV
E	70,451	60,937	64,807[a]	MPa
σ_y	287.5	60.9	153.0[a]	MPa
σ_u	308.8	119.1	196.3[a]	MPa
K'	459.7	230.4	316.0[a]	MPa
n'	0.07	0.16	0.11[a]	—

[a]Estimated on the basis of Vickers hardness.

J. Bridge Eng. 2012.17:409-419.

cross-section in the vicinity of the weld, including both the 5356 aluminum weld metal and the 6061 base metal in the HAZ, as shown in Fig. 7(a). Average HV numbers of 86.6 and 74.8 were obtained for the weld metal and HAZ, respectively, suggesting that their material properties lie between those of the T651 and O temper base metal.

Estimation of HAZ Mechanical Properties

Given the material properties of the T651 and O temper base metal, along with the hardnesses of the T651 and O temper base metal and the HAZ, the material properties of the HAZ were estimated on the basis of Baumel and Seeger (1990), wherein it is proposed that the cyclic Ramberg-Osgood material constants for aluminum can be estimated as follows:

$$K' = 1.61 \cdot \sigma_u \quad \text{and} \quad n' = 0.11 \tag{5}$$

Baumel and Seeger (1990) provide a linear relationship between hardness and ultimate strength for steel, but not for aluminum. With no such relationship, the ultimate strength (σ_u) of the HAZ was estimated by linear interpolation. In view of the lack of a viable alternative, and because the only difference between the three materials (as-received, annealed base metal, and HAZ) was the thermal history, this approach was thought to be reasonable. Estimation of the elastic modulus (E) and yield strength (σ_y) of the HAZ was performed in a similar manner. The resulting estimated HAZ material properties are provided in Table 2.

Residual Stress Measurements

X-ray diffraction measurements of the residual stresses along the expected crack path were performed by Proto Manufacturing, in accordance with ASTM (2002) and the Society of Automotive Engineers International (SAE 2003), at two locations on a single specimen. Along with surface measurements, subsurface measurements were obtained by electropolishing. The results are summarized in Fig. 7(b). The maximum tensile residual stress at a depth of 0.5 mm is 41 MPa, or ~15% of σ_y (T651).

Fracture Mechanics Analysis of Fatigue Specimens

Given the lack of test data under VA loading, fracture mechanics analysis has historically been a primary means for justifying the use of a multislope S-N curve for VA loading design of aluminum fatigue details beyond the CAFL in some standards (Menzemer 2000). In Menzemer (1992), such an analysis is presented. Constant, linear, and Rayleigh VA loading spectrums are analyzed in this reference. The results show that the S-N curve for VA loading conditions may have two slopes. However, the difference in the slopes diminishes with the introduction of periodic overload cycles. In general, the slope of the S-N curve for VA loading design will be dependent on the characteristics of the VA loading spectrum. With this in mind, the following sections present a fracture mechanics analysis of aluminum welds conducted with the specific purpose of examining the S-N curve shape for an aluminum fatigue detail under a broad range of in-service VA loading conditions typical of North American highway bridges.

Strain-Based Fracture Mechanics Model

The strain-based fracture mechanics (SBFM) model employed in this investigation is a large crack fracture mechanics model, adapted to account for nonlinear material and short crack behavior on the basis of previous publications (El Haddad et al. 1979; Dabayeh et al. 1998; Khalil and Topper 2003). As demonstrated by Ghahremani and Walbridge (2011) for steel welds, this model is capable of accurately predicting fatigue behavior under in-service VA bridge loading conditions. Under conditions expected to result in a linear material response, its predictions converge on those obtained by using linear elastic fracture mechanics (LEFM). According to the model, fatigue life is calculated by using the Paris-Erdogan crack growth law, modified to consider crack closure effects and a threshold stress intensity factor (SIF) range, ΔK_{th}, and integrated over a crack depth range, a_i to a_c

$$N = \int_{a_i}^{a_c} \frac{da}{C \cdot \max(\Delta K_{\text{eff}}^m - \Delta K_{\text{th}}^m, 0)} \tag{6}$$

where C and m are constants. The effective stress intensity factor range, ΔK_{eff}, considering crack closure (or opening) effects, is determined by the following expression:

$$\Delta K_{\text{eff}} = K_{\max} - \max(K_{op}, K_{\min}) \tag{7}$$

where $K_{\max}$ and $K_{\min}$ are the SIFs attributable to the maximum and minimum local strain levels (ε) for each load cycle; and K_{op} = SIF corresponding with the crack opening strain level for a given load cycle. The following expression is used to calculate each SIF:

$$K = Y \cdot E \cdot \varepsilon \cdot \sqrt{\pi \cdot (a + a_0)} \tag{8}$$

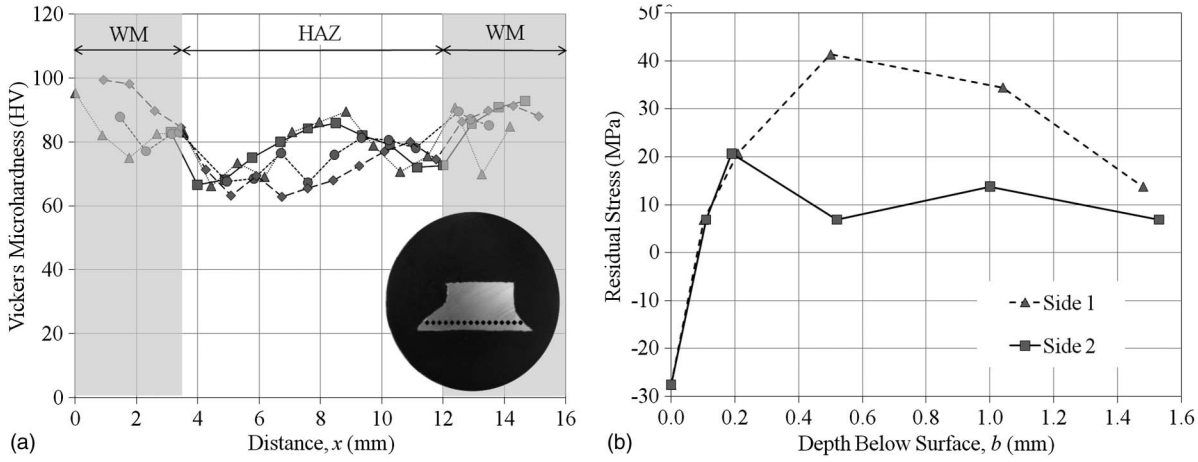

Fig. 7. Microhardness and residual stress measurements: (a) microhardness measurements; (b) residual stress measurements

J. Bridge Eng. 2012.17:409-419.

where a_0 = material constant to account for small crack behavior; and Y = correction factor to account for the crack shape, the free surface on one side of the crack, and the finite thickness of the cracked plate. The constant a_0 can be taken as (El Haddad et al. 1979)

$$a_0 = \left(\frac{\Delta K_{th}}{\Delta \sigma_e}\right)^2 \cdot \frac{1}{\pi} \tag{9}$$

where $\Delta\sigma_e$ = fatigue limit for $R = -1 (\approx 0.5 \cdot \sigma_u)$. A Ramberg-Osgood material model is used to calculate the stresses and strains for each load cycle. Local stress-strain histories at various depths below the surface of the weld notch are determined by using Neuber's rule. The local elastic stresses (σ_{el}) are calculated by using a stress concentration factor (SCF), $k_p (= \sigma_{el}/S)$, which accounts for the presence of the crack (Dabayeh et al. 1998)

$$k_p = \frac{K_{el}}{Y \cdot \sqrt{\pi \cdot a}} \tag{10}$$

where K_{el} = elastic SIF, accounting for the nonuniform stress distribution along the crack path, and is calculated by using weight functions, m (b, a, c), from Shen and Glinka (1991). For the calculation of ΔK_{eff}, the crack opening stress is calculated on the basis of Newman (1984). For VA loading analysis, the following expression from Khalil and Topper (2003) is used to model the evolution of the crack opening stress (σ_{op}) following overload events:

$$\sigma_{op} = \sigma_{cu} + \mu \cdot (\sigma_{ss} - \sigma_{cu}) \tag{11}$$

where σ_{cu} = crack opening stress before the current cycle; σ_{ss} = crack opening stress at steady state (i.e., under CA loading at the current stress range); and μ = material constant, found to equal 0.003 for 2024-T351 aluminum (Khalil and Topper 2003). Further details regarding the employed SBFM model are provided by Ghahremani and Walbridge (2010).

Assumed Model Input Parameters

To implement the SBFM model described in the previous section, the estimated HAZ material parameters in Table 2 were assumed for the elastic modulus, E, static yield and ultimate strength, σ_y and σ_u, and the Ramberg-Osgood material constants, K' and n'.

To determine the local (applied) elastic stresses, σ_{el}, a 2D (plane strain) analysis of the uncracked weld specimen was performed by using the finite-element (FE) program ABAQUS 6.7.4 (ABAQUS 2007). Nominal specimen dimensions were assumed, along with a weld toe angle and radius of $\theta_w = 45°$ and $\rho = 0.5$ mm, respectively. In Fig. 8, the FE mesh and boundary conditions are illustrated and the resulting uncracked SCF (k_{el}) and k_p distributions are plotted. A critical crack depth of $T/2$ was assumed, where T is the nominal plate thickness.

To model the evolution of the crack shape with depth, an empirical model from Menzemer (1992) was employed, wherein the crack half-width, c, is calculated as

$$c = 3.274 \cdot a^{1.241} \tag{12}$$

Crack shape measurements were obtained from the fatigue test specimens by dye penetrant staining following crack detection (Coughlin 2010). These measurements showed considerable scatter ($a/c = 0.133$ to 0.366 for $a > 3.0$ mm) with no clear correlation between the crack shape and either the crack depth or loading case. A reasonable estimate is given by Eq. (12) of the mean crack shape at the higher crack depths where a/c measurements were obtained.

For the fracture mechanics analysis of aluminum, a multislope crack growth rate (da/dN) curve is commonly used. Because the crack opening SIF is considered explicitly in the SBFM model, an effective SIF versus da/dN curve is needed. Menzemer (1992) recommends that da/dN data obtained under constant K_{max} or high R-ratio conditions are used in this case. The European Committee for Standardization (CEN 2007) provides a set of curves for various wrought aluminum alloys on the basis of a combination of constant K_{max} conditions at low SIFs and $R = 0.8$ at high SIFs. In Fig. 9, along with an envelope of these curves, curves for Al-Mg-Si alloys from the following references are compared: R84 (Ruschau 1984), K08 (Kim et al. 2008), D99 (Donald and Paris 1999), B01 (Borrego et al. 2001), and EC9 (CEN 2007). With no batch-specific data available, it was decided to employ an SIF versus da/dN curve on the basis of the upper bound of the curves in Fig. 9(a).

Taylor (1985) reported values ΔK_{th} ranging from 22.1 to 94.9 MPa/mm for $R > 0.4$ for various aluminum alloys. In this paper, a value for this parameter of 1.0 MPa/m (or 31.6 MPa/mm) is used, which is a common assumption for aluminum. This value is at the lower end of the range reported by Taylor (1985) and results in a good fit of the test data at longer lives.

Initial defect measurements for aluminum welds performed with a scanning electron microscope are reported by Menzemer (1992). In this reference, a mean defect depth, a_i, of 0.025 mm is reported,

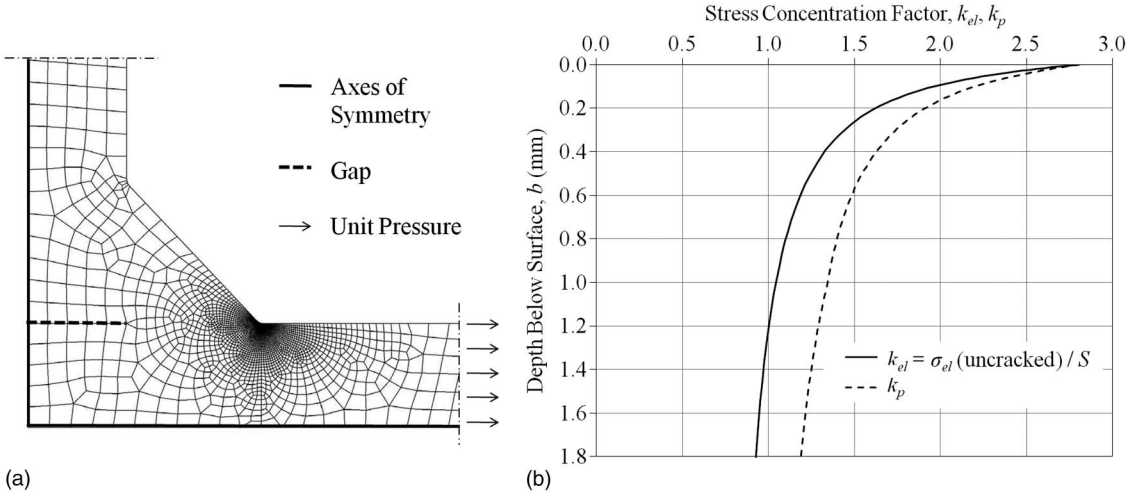

Fig. 8. Determination of stress concentration factors: (a) finite-element model of weld detail; (b) resulting stress concentration factor distributions

J. Bridge Eng. 2012.17:409-419.

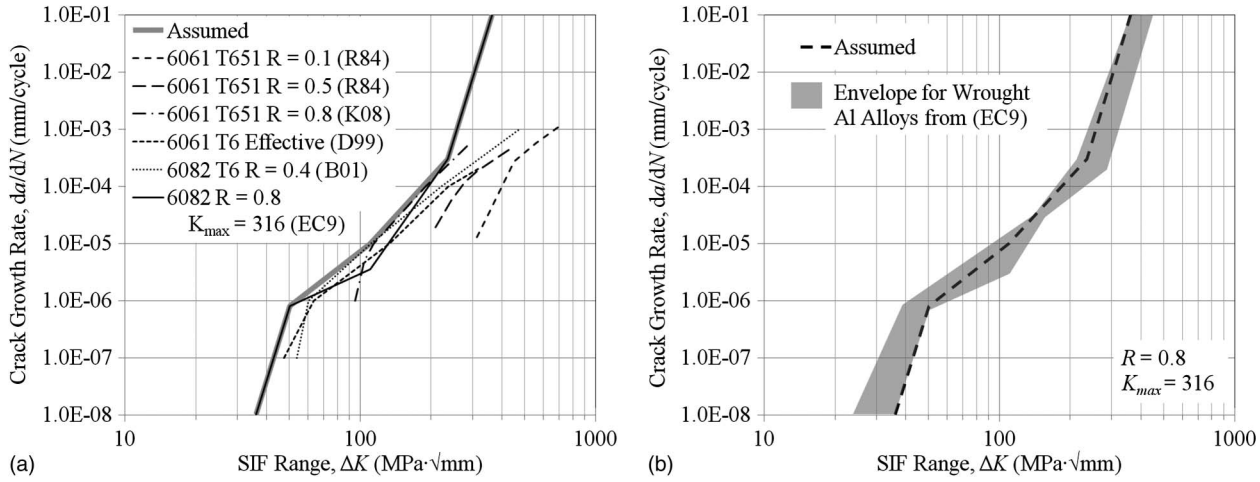

Fig. 9. Crack growth data for aluminum alloys: (a) Al-Mg-Si alloys; (b) other wrought aluminum alloys

with depths ranging from 0.013 to 0.051 mm. These depths are smaller than the values reported elsewhere for structural steel welds. In Maddox and Webber (1977), fracture mechanics is used to back calculate an effective initial defect depth for aluminum welds. On the basis of this approach, an a_i value ~1/10 as large as the value for steel is estimated.

For the current study, the high uncertainty regarding the expected initial defect depth and residual stress distribution were handled as follows: these parameters were initially set to $a_i = 0.025$ mm [the mean measured value reported by Menzemer (1992)] and $\sigma_{res} = 20$ MPa [rounded mean measured value in Fig. 7(b)]. A uniform residual stress distribution was simplistically assumed; then, a_i was varied to determine the best value for predicting the CA loading results for $R = 0.1$ and 0.4, on the basis of a least squares comparison with the test data. This yielded a calibrated value of $a_i = 0.04$ mm. Simulations of the other tested loading conditions were then performed with $a_i = 0.04$ mm and σ_{res} varied from 0 to 40 MPa, so that the sensitivity of the results to the assumed uniform residual stress level could be observed.

Validation of Strain-Based Fracture Mechanics Model

In Fig. 10, the test results and SBFM model predictions are compared for the CA and VA loading tests. The CA results show that good predictions are achieved for the various tested stress ranges and ratios. The variations in σ_{res} between 0 and 40 MPa provide an explanation for the increased scatter in the CA loading results for $R = -1.0$, assuming that $\sigma_{res} = 20$ MPa gives a good prediction of the expected life for all three stress ratios.

Under simulated in-service VA loading conditions, the tested and predicted fatigue lives also compare reasonably well for both investigated load histories. Specifically, several important trends are predicted by the analytical model, including the higher fatigue strength at 10^5 cycles observed for the ps-m-40 history, and the higher fatigue life predicted for this load history in the high-cycle domain. The model predictions are on the safe side for the ps-m-40 load history. For the ps-r-15 history, a reasonably good fit of the test data is observed.

Analytical Studies Performed with Validated Fracture Mechanics Model

Simulations for Other Spans and Influence Lines

Following the SBFM model validation, simulations were conducted to generate analytical S-N curves for loading histories applicable to other influence lines and bridge spans. Specifically, influence lines for the following five locations were considered:

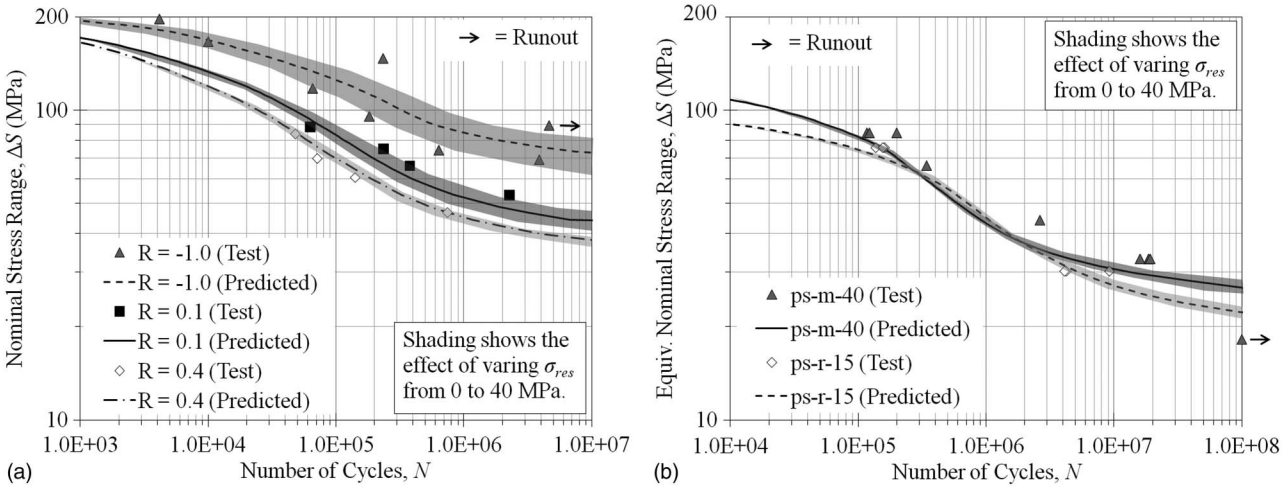

Fig. 10. Strain-based fracture mechanics model predictions compared with fatigue test data: (a) CA loading; (b) VA loading

midspan moment for 1- and 2-span girders (ps-m, p2tr-m); intermediate support moment for 2-span girders (p2tr-a); and support reactions for 1- and 2-span girders (ps-r and p2tr-r). The following four bridge spans were considered: 15, 25, 40, and 60 m. The selected influence lines and spans were not intended to reflect the most likely cases for fatigue cracking in highway bridges, but rather to cover a broad range of load history characteristics that can be expected in these structures. To generate each in-service loading history, random samples of 1,000 trucks taken from the two previously-described larger U.S. and Ontario databases were used.

In Fig. 11, the analysis results are presented for both the U.S. and Ontario loading simulations. In this figure, the results are plotted as envelopes in terms of both the equivalent stress range, ΔS_{eq}, on the basis of Eq. (4) and the design stress range, $\gamma\Delta f$ or λf_{sr}. For both stress range types, the ADM (AA 2010) detail category C S-N curve slope ($m = 3.64$) is assumed. In the second case, the assumed values for γ or λ are the mean values plotted in Fig. 3(b).

In Fig. 11, the ADM (AA 2010) detail category C design S-N curve and the analytical S-N curve for CA loading at $R = 0.1$ are plotted for comparison purposes. The results show that the ADM (AA 2010) design curve lies below the VA loading envelopes for the most part. When the equivalent stress range (ΔS_{eq}) is used, the model predicts fatigue strengths for $N < 10^5$ cycles below the design curve for a significant number of the analyzed cases. However, when the design stress ranges are used, the envelopes shift upwards for $N < 10^5$ cycles, and the ADM (AA 2010) design curve is generally safe in this domain.

Considering the widths of the VA loading envelopes in Fig. 11 and comparing the differences in the envelopes for the two investigated GVW databases, it is clear that the in-service VA loading characteristics have a significant influence on the shape of the analytical VA loading S-N curve. In general, the VA loading envelopes suggest that a flatter design S-N curve slope may be warranted in the high cycle domain. A number of factors influencing this result must be further studied, because of the following: (1) large uncertainties remain regarding certain key model parameters, and (2) the model has so far been validated on small-scale test data only.

Scale Effect and Overload Studies

In Fig. 12, results are presented to illustrate the following effects on the VA loading envelopes: (1) varying several model parameters

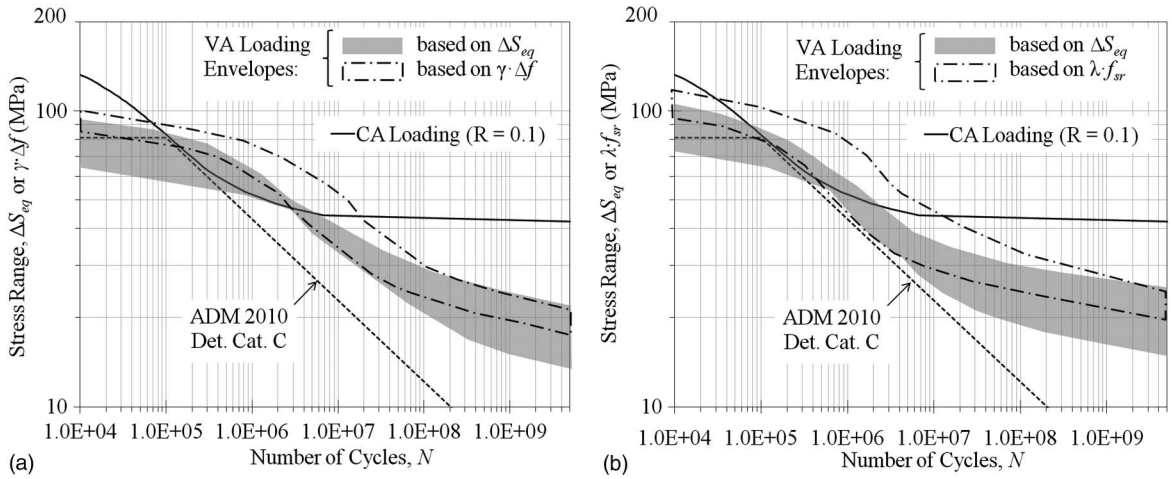

Fig. 11. Results of analysis of other spans and influence lines: (a) U.S. gross vehicle weight data; (b) Ontario gross vehicle weight data

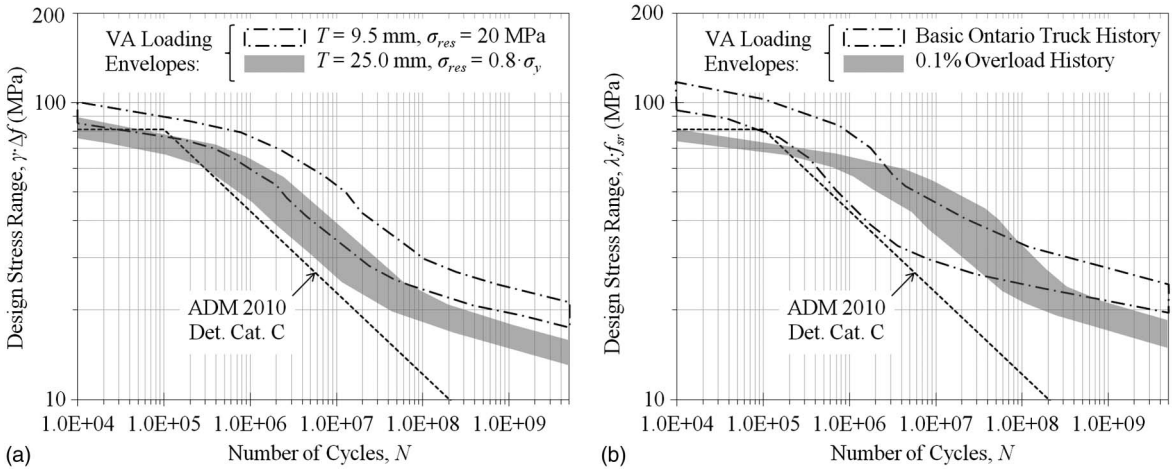

Fig. 12. Scale effect and overload study results: (a) scale effect study results (U.S. gross vehicle weight data); (b) overload study results (Ontario gross vehicle weight data)

J. Bridge Eng. 2012.17:409-419.

often used to explain "scale effects," and (2) introducing a particularly heavy truck at a regular frequency in the traffic history.

Fig. 12(a) shows that a new VA loading envelope is generated for a weld detail identical to the one described previously, but with the thickness of the loaded plate increased to $T = 25.0$ mm. This results in an increase in the SCF along the crack path. In addition, the residual stress is increased to a level more typical of full-scale structures. Kosteas (1988) and (Menzemer (1992) reported that they have measured residual stresses in large-scale specimens of up to ~50% or 80% of the parent material yield strength, respectively. For this study, the higher value of 80% of σ_y is assumed. The result of this analysis is a downward shift in the VA loading envelope.

In Fig. 12(b), a new VA loading envelope is produced for the Ontario GVW database, with an overload truck introduced every 1000th truck, which has an axle configuration identical to the CAN/CSA-S6 CL-625 truck and the corresponding axle loads multiplied by 1.5, resulting in a GVW of 93.75 kN. The addition of this overload truck results in a downward shift in the VA loading envelope in the high and low cycle domains. In between these domains, an upward shift in the envelope can be seen, which can be explained by the well-known beneficial "crack growth retardation" effects of tensile overload cycles under certain conditions.

Conclusions

On the basis of the work presented in this paper, the following conclusions are drawn:

- The damage equivalence factors currently specified in AASHTO (2007) and CAN/CSA-S6 (CSA 2006) for steel do not necessarily provide the same level of safety when used with aluminum S-N curves. The difference is most significant for ADM (AA 2010) detail categories *A* and *B*, or *m* greater than ~4.5. On this basis, it is concluded that higher factors may be appropriate in these cases to ensure a level of safety consistent with the current provisions for steel.
- A validated deterministic fracture mechanics model indicates that the ADM (AA 2010) detail category *C* S-N curve for aluminum provides safe fatigue performance predictions for the investigated fatigue detail in both the low and high-cycle domains.
- This model predicts a slope change in the calculated S-N curve envelopes for various bridge spans and influence lines under in-service VA loading in the high-cycle domain, which could potentially be exploited to reduce the fatigue design stress for aluminum highway bridges. This slope change shifts downwards, however, when several parameters associated with scale effects and the in-service VA loading history are varied.

In addition, the following recommended areas of further study are highlighted:

- A more extensive analysis of the damage equivalence factors for aluminum is recommended, employing larger, more recent traffic databases and considering the effects of periodic overload trucks and simultaneous vehicle crossings in the analysis.
- Further study is still needed to fully understand all of the issues concerning the fatigue behavior of aluminum welds under in-service highway bridge loading conditions. Although additional VA loading tests of large-scale components and other fatigue details will be essential, the methodology employed in this paper can be used to identify critical loading histories for testing and to predict fatigue behavior for untested details and loading histories, to reduce the cost of a comprehensive test program.
- For the development of future design S-N curves or further verification of the existing ones, conversion of the described analysis methodology into a probabilistic format would provide a means for establishing curves corresponding with a consistent reliability level, given the limited available test data under in-service VA loading conditions.

Acknowledgments

Funding for this project was provided by the Ontario Graduate Scholarship (OGS) program and the Natural Sciences and Engineering Research Council of Canada (NSERC). Assistance with laboratory testing was provided by M. El Zeghayar and K. Ghahremani. Technical input provided by A. Agarwal, D. Beaulieu and the other members of CAN/CSA-S6 Technical Sub-Committee on Section 17—Aluminum Structures, is gratefully acknowledged.

References

ABAQUS. (2007). *Version 6.7.4 user documentation*, Dassault Systems.

Agarwal, A. C. et al. (2007). *Calibration report for CAN/CSA-S6-06*, Canadian Standards Association, Mississauga, ON.

Aluminum Association (AA). (2010). "Aluminum design manual—specifications and guidelines for aluminum structures." *ADM-10*, Aluminum Association, Arlington, VA.

AASHTO. (2007). *AASHTO LRFD bridge design specification*, 4th Ed. AASHTO, Washington, DC.

ASTM. (2002). "Standard test method for verifying the alignment of x-ray diffraction instrumentation for residual stress measurement." *ASTM E915*, West Conshohoken, PA.

ASTM. (2003). "Standard test method for vickers hardness of metallic materials." *ASTM E92-82*, West Conshohoken, PA.

ASTM. (2004). "Standard test methods for tension testing of metallic materials." *ASTME8M-04*, West Conshohoken, PA.

ASTM. (2009). "Standard practice for heat treatment of wrought aluminum alloys." *ASTM B 918M-09*, West Conshohoken, PA.

Arrien, P., Bastien, J., and Beaulieu, D. (2001). "Rehabilitation of bridges using aluminum decks." *Can. J. Civ. Eng.*, 28, 992–1002.

Baumel, A., and Seeger, T. (1990). *Materials data for cyclic loading—Supplement 1*, Elsevier Science Publishing, New York.

Borrego, L. P., Ferreira, J. M., and Costa, J. M. (2001). "Fatigue crack growth and crack closure in an AlMgSi alloy." *Fatigue Fract. Eng. Mater. Struct.*, 24(4), 255–265.

Canadian Standards Association(CSA). (2005). "Strength design in aluminum." *CSA-S157-05*, Mississauga, ON, Canada.

Canadian Standards Association (CSA). (2006). "Canadian highway bridge design code." *CAN/CSA-S6-06*, Mississauga, ON, Canada.

Coughlin, R. (2010). "Fatigue of aluminum welds in canadian highway bridges." M.A.Sc. thesis, Univ. of Waterloo, Waterloo, ON.

Dabayeh, A. A., Berube, A. J., and Topper, T. H. (1998). "An experimental study of the effect of a flaw at a notch root on the fatigue life of cast Al 319." *Int. J. Fatigue*, 20(7), 517–530.

Das, S. K., and Kaufman, J. G. (2007). *Aluminum alloys for bridges and bridge decks*, The Minerals, Metals & Materials Society, Warrendale, PA, 61–72.

Donald, K., and Paris, P. C. (1999). "An evaluation of ΔK_{eff} estimation procedures on 6061-T6 and 2024-T3 aluminum alloys." *Int. J. Fatigue*, 21(1), 47–57.

El Haddad, M. H., Topper, T. H., and Smith, K. N. (1979). "Prediction of non propagating cracks." *Eng. Fract. Mech.*, 11, 573–584.

European Committee for Standardization (CEN). (2007). "Eurocode 9—design of aluminium structures—part 1-3: Structures susceptible to fatigue." *EN 1999-1-3*, Brussels, Belgium.

Ghahremani, K., and Walbridge, S. (2011). "Fatigue testing and analysis of peened highway bridge welds under in-service variable amplitude loading conditions." *Int. J. Fatigue*, 33(3), 300–312.

Hirt, M. A., Bez, R., and Nussbaumer, A. (2006). *Traite de génie civil Vol. 10: Construction métallique—Notions fondamentales et méthodes de dimensionnement*, Presses Polytechniques et Universitaires Romandes, Lausanne Switzerland (in French).

Hobbacher, A. (2005). "Recommendations for fatigue design of welded joints and components." *Doc. XIII-1965-03*, International Institute of Welding (IIW), Villepinte, France.

Jaccard, R., Kosteas, D., and Ondra, R. (1995). "Background document to fatigue design curves for welded aluminium components." *Doc. XIII-1588-95*, International Institute of Welding (IIW), Villepinte, France.

Khalil, M., and Topper, T. H. (2003). "Prediction and correlation of the average crack-opening stress with service load cycles." *Int. J. Fatigue*, 25, 661–670.

Kim, S., Lee, C. G., and Kim, S.-J. (2008). "Fatigue crack propagation behavior of friction stir welded 5083-H32 and 6061-T651 aluminum alloys." *Mater. Sci. Eng. A*, 478(1–2), 56–64.

Kosteas, D. (1988). "Estimating residual stresses and their effect in welded aluminum components in fatigue." *ASTM Special Technical Publication STP 1004*, West Conshohocken, PA, 122–130.

Maddox, S. J., and Webber, D. (1977). *Fatigue Crack Propagation in Aluminum-Zinc-Magnesium Alloy Fillet-Welded Joints*, *ASTM Special Technical Publication STP 648*, West Conshohocken, PA, 159–184.

Maddox, S. J. (1995). "Scale effect in fatigue of fillet welded aluminium alloys." *Proc. 6th Int. Conf. on Aluminium Weldments*, American Welding Society, Miami, FL, 77–94.

Maddox, S. J. (2003). "Review of fatigue assessment procedures for welded aluminium structures." *Int. J. Fatigue*, 25(12), 1359–1378.

Mazzolani, F., and Grillo, M. (1995). "Fatigue strength of longitudinally welded aluminium alloy structures." *Proc. 6th Int. Conf. on Aluminium Weldments*, American Welding Society, Miami, FL, 95–106.

Menzemer, C. C. (1992). "Fatigue behavior of welded aluminum structures." Ph.D. thesis, Lehigh Univ., Bethlehem, PA.

Menzemer, C. C., and Fisher, J. W. (1995). "Revisions to the aluminum association fatigue design specifications." *Proc. 6th Int. Conf. on Aluminium Weldments*, American Welding Society, Miami, FL, 11–23.

Menzemer, C. C. (2000). "Fatigue behaviour and design of aluminum structures." *Prog. Struct. Eng. Mater.*, 2, 120–127.

Moses, F., Schilling, C. G., and Raju, K. S. (1987). "Fatigue evaluation procedures for steel bridges." *National Cooperative Highway Research Program Rep. 299*, Washington, DC.

Newman, J. C. (1984). "A crack opening stress equation for fatigue crack growth." *Int. J. Fract.*, 24, R131–R135.

Ruschau, J. J. (1984). *Fatigue crack growth rate data for aluminum alloy 6061-T651 plate, Dayton Univ. Research Institute Interm Technical Rep.*, Dayton, OH.

Shen, G., and Glinka, G. (1991). "Weight functions for a surface semi-elliptical crack in a finite thickness plate." *Theor. Appl. Fract. Mech.*, 15(3), 247–255.

Siwowski, T. (2006). "Aluminum bridges—past, present and future." *Struct. Eng. Int.*, 16(4), 286–293.

Snyder, R. E., Likins, G. E., and Moses, F. (1985). "Loading spectrum experience by bridge structures in the united states." *Federal Highway Administration Rep., FHWA/RD-85/012*, Cleveland, OH.

Society of Automotive Engineers International (SAE). (2003). "Residual stress measurement by x-ray diffraction." *SAE HS784*, Warrendale, PA.

Soetens, F., van Straalen, I. J., and Dijkstra, O. (1995). "European research on fatigue of aluminium structures." *Proc. 6th Int. Conf. on Aluminium Weldments*, American Welding Society, Miami, FL, 53–64.

Swiss Society of Engineers and Architects (SIA). (2003). "Steel structures." *SIA 263*.

Taylor, D. (1985). "A compendium of fatigue thresholds and crack growth rates." EMAS, Warley, U.K.

Voutaz, B., Smith, I. F., and Hirt, M. A. (1995). "Fatigue behaviour of aluminium beams with welded attachments." *3rd Int. Conf. on Steel and Aluminium Structures*, Dept. of Civil Engineering, Bogazici Univ., Istanbul, Turkey, 213–220.